Supporting information

From low to high density: the effect of ionic modifications on permselectivity in biimidazole-based polyimides

Alain Tundidor-Camba[a*], Ifeanyi S. Ibeto[a], Yennier Cruz[b], Fidel E. Rodriguez-Gonzalez[b], Pravin S. Shinde[a], Ana L. Montero-Alejo[c], Claudio A. Terraza[b,d], Sree Laxmi[e], Akhilesh Upasani[e], Sergey Vasenkov[e], Joshua D. Moon[e], Kathryn E. O'Harra[a], C. Heath Turner[a], and Jason E. Bara[a*]

[a]*Department of Chemical & Biological Engineering, The University of Alabama, Tuscaloosa, Alabama 35487-0203, United States.*

[b]*Research Laboratory for Organic Polymers (RLOP), Department of Organic Chemistry, Pontificia Universidad Católica de Chile, Santiago 7820436, Chile.*

[c]*Departamento de Física, Facultad de Ciencias Naturales, Matemática y del Medio Ambiente (FCNMM), Universidad Tecnológica Metropolitana, Santiago 7800003, Chile.*

[d]*UC Energy Research Center, Pontificia Universidad Católica de Chile, Santiago 7820436, Chile.*

[e]*Department of Chemical Engineering, University of Florida, Gainesville, Florida 32611, United States.*

Email: atundidorcamba@ua.edu; jbara@eng.ua.edu

TABLE OF CONTENT

MATERIALS AND METHODS

Materials

Anhydrous *N*,*N*-dimethylacetamide (DMAc), anhydrous pyridine (Py), anhydrous acetic anhydride (Ac_2O), 6FDA, 3,3-dibromo-1,1,1-trifluoropropan-2-one (98%) and terephthalaldehyde (98%) were purchased from AKScientific. 6FDA was sublimated before use. 4-Nitro-1-fluorobenzene (98%), MeI (99%) and palladium supported on activated carbon (Pd/C, 10 wt. %) were purchased from BeanTown Chemical. Lithium bis(trifluoromethanesulfonyl)imide ($LiNTf_2$) (99%) was purchased from IoLiTec. [C_4mim][Tf_2N] (IL) was previously prepared for our research group according to well-established procedures[1–3]. All other reagents and solvents were purchased commercially as analytical grade and used without further purification.

Characterizations

FTIR spectra were obtained using a PerkinElmer Spectrum 2 with an attenuated total reflectance (ATR) accessory over the range of 4000 - 450 cm^{-1}. ^1H and ^{13}C NMR spectra were carried out on a 500 MHz instrument (BRUKER AV500) using DMSO-d_6 as solvents and TMS as internal standard. The density of the films was determined from the Archimedes' principle using a top loading electronic Mettler Toledo GmBH balance and density kit using heptane. Differential scanning calorimetry (DSC) was conducted on a TA Instruments DSC Q2000 at a heating rate of 10 °C min^{-1} under a N_2 atmosphere. Thermogravimetric analysis (TGA) was performed on a TGA7 thermogravimetric analyzer (PerkinElmer Inc., USA) under N_2 atmosphere with a heating rate of 20 °C min^{-1} from 50 °C to 800 °C. The tensile properties of the film were performed using a uniaxial testing machine (Shimadzu EZ-LX) under a strain rate of 5 mm/min at room temperature. The film was cut in rectangular strips (5 cm long, 0.5 cm wide and 0.085 mm thick). An average of three individual measurements was used for statical purposes. Wide-angle X-ray diffraction (WAXD) was conducted using a Bruker D8 Discover instrument equipped with a general area detector diffraction system with CoKα radiation (wavelength λCo = 1.790 Å), in a 3 – 60° 2θ range. The average *d*-spacing was calculated using Bragg's law (Eqn.1):

$$d = \frac{n\lambda}{2sin\theta} \qquad eq\ 1$$

where θ was assigned from the broad, amorphous peak maximum[4]. Pure gas permeability coefficients (*P*) were determined using a constant volume permeation cell of the type described elsewhere at 35 °C,[5] according to Eqn 2:

$$P = \frac{273\ \ Vl\ \ dp}{76\ ATp_0 dt} \qquad eq\ 2$$

where A and l are, the effective area and the thickness of the film, respectively. T is the temperature of the measurement (308.15 K), V is the constant volume of the permeate cell, p_0 is the pressure of the feed gas in the upstream, and dp/dt is the gas pressure increase with time under steady-state conditions measured in the permeate cell. P is expressed in Barrer [1 Barrer = 10^{-10} [cm^3 (STP) cm cm^{-2} s^{-1} $cmHg^{-1}$]. The downstream pressure was maintained at 10^{-2} mbar, while the upstream pressure was kept, for all gases, at 2 bar. For the permeation experiments pure gases, hydrogen (H_2), oxygen (O_2), nitrogen (N_2), carbon dioxide (CO_2), and methane (CH_4) were used. The purities for CH_4 and O_2 were greater than 99.95% and for the other gases were greater than 99.99%.

Then, the ideal selectivity $\alpha_{i,j}$ of a membrane for the separation of a gas pair mixture was calculated as the ratio of each pure gas permeability:

$$\alpha_{i,j} = \frac{P_i}{P_j} = \frac{S_i}{S_j} \cdot \frac{D_i}{D_j} \qquad eq\ 3$$

CO_2 and CH_4 solubilities for each membrane were measured using the dual volume pressure decay method[5]. The polymer samples were placed into the sample chamber inside a water bath which was kept at a constant temperature of 35 °C. Samples were held under vacuum for 16 hours to allow adequate degassing before every experiment. Blank experiments (no polymer) were performed using non-sorbing stainless steel ball bearings to account for any gas adsorption onto the apparatus itself[6]. Software from Maxwell Robotics along with an Omega pressure transducer were used for data collection. Eq. 6 was used to calculate the moles of gas sorbed into the polymer for each pressure step used during the sorption experiment:[7]

$$n = \sum_{i=1}^{m} \frac{1}{RTZ_i} * \left(P_{C,i} - P_{eq,i}\right) * (V_c + V_S) \qquad eq\ 4$$

where n is the total number of moles of gas sorbed, m is the number of pressure steps, R is the ideal gas constant in units of $\left[\frac{psi\ cm^3}{mol\ K}\right]$, T is temperature $[K]$, P_C is the charge pressure $[psi]$, V_C is the charge volume $[cm^3]$, P_{eq} is the pressure at sorption equilibrium $[psi]$, V_s is the sample chamber volume which accounts for the volume of the polymer sample $[cm^3]$, and Z is the compressibility factor at the equilibrium pressure calculated using the third virial coefficient[8] for each gas (CO_2/CH_4). For all the measurements, experimental uncertainties were calculated using propagation of errors as described in Johnson *et al.*[9] The sorption isotherms can be used to calculate thermodynamic factors (α) which represent an additional "thermodynamic driving force" for transport. The thermodynamic factor is calculated from the isotherms as follows:

$$\alpha = \frac{d\ln p}{d\ln c} = \frac{c}{p} * \frac{\partial p}{\partial c} \qquad eq\ 5$$

Pulsed field gradient (PFG) NMR diffusion experiments were performed to determine the self-diffusivities of sorbed gases in each membrane. To prepare each NMR sample, a membrane was cut into thin strips with a width of 2 to 3 mm and a length of 1 to 3 cm which were inserted into a 5 mm medium-wall NMR tube (Wilmad Labglass, Inc.). The membrane strips in the NMR tube were arranged such that the length of the strip was aligned parallel to the axis of the tube. The total mass of membrane strips per NMR sample ranged from 70 to 95 mg. The NMR tubes containing membrane samples were connected to a custom-made vacuum system, gradually heated under vacuum to 100°C, and maintained at this temperature for 8 hours to remove residual moisture. After activation, the samples were allowed to cool to room temperature (~25°C) while still under vacuum and cryogenically loaded using liquid nitrogen with a desired amount of either one-component gas or two-component gas mixture. ^{13}C-labeled CO_2 and ^{13}C-labeled CH_4 (all 99% isotopic purity, Sigma-Aldrich) were used as sorbates. After gas loading, the NMR tubes were flame sealed and separated from the vacuum system. In all cases, the amount of gas loaded corresponded to the total equilibrium gas loading pressure of around 10 bar under the measurement conditions. The equilibrium gas loading pressure of 10 bars used for PFG NMR was significantly higher than the gas pressure used in the permeation measurements at the membrane inlet (2 bars). The higher gas pressure used for the PFG NMR measurements was necessary to achieve sufficiently high signal-to-noise ratios in these measurements. Prior to NMR measurements, the NMR tubes containing the samples were kept at the measurement temperature inside the NMR spectrometer for a minimum of 30 minutes to achieve a sorption equilibrium. Following this equilibration time selected identical NMR measurements were performed periodically over the course of 2 to 3 hours. An observation of no change in the measured NMR data indicated that the equilibrium time was sufficiently long.

The gas loading pressure and intra-membrane concentrations in each NMR sample were estimated in the same way as in our previous studies[10,11] by using the proportionality between the area under the gas NMR spectrum and the number of gas molecules corresponding to this spectrum. The contributions to the NMR signal from the gas inside membrane strips in a sample and the gas phase between these strips were calculated separately based on a mass balance approach using the following known properties: a) total volume of the NMR tube, b) total volume of the membrane sample, and c) total mass of the gas loaded in the NMR tube. This allowed obtaining gas concentrations inside the membrane strips and in the surrounding gas phase. The equilibrium gas loading pressure in each sample was determined using the gas concentration and temperature in the gas phase and applying the known equation of state[12,13]. The gas loading pressures and intramembrane gas concentrations in the measured samples are presented in Tables S1-S3. For the two-component gas mixture samples,

the partial pressures of ~7 bar of CO_2 and ~3 bar of CH_4 were selected to maintain the same total gas pressure and similar total intramembrane gas concentration as in the one-component CO_2 samples. NMR experiments were conducted using an Avance III 14 T/51 mm spectrometer (Bruker Biospin), which operates at a frequency of 149.8 MHz for ^{13}C nuclei and 600 MHz for ^{1}H nuclei. The NMR measurements were performed using ^{13}C nuclei for CO_2, while ^{1}H nuclei were primarily used for CH_4. In addition, selected NMR diffusion measurements employing ^{13}C nuclei were also carried out for CH_4 to confirm the consistency of results and to rule out any potential experimental artifacts. The magnetic field gradient pulses were generated using *DiffBB* diffusion probe (Bruker Biospin). Sinusoidal-shaped magnetic field gradient pulses with amplitudes g ranging from 0.3 to 17 T/m and effective gradient pulse durations (δ) of 0.5 – 1.3 ms were used. The time between consecutive scans was set within the range of 3 – 4 s, which was at least 1.5 times larger than the T_1 NMR relaxation time. Diffusion coefficients were determined for each sample at various effective diffusion times, t_{eff}, which is the time of observation of the diffusion process, ranging from 20 to 500 ms. Longitudinal eddy current (LED) delay of 6 ms was used. Each diffusion experiment at a given t_{eff} was performed twice, and the final diffusion data were obtained by averaging the results from these two measurements. To measure a single self-diffusivity, the overall data acquisition time varied between 1.5 and 6 h.

To determine the self-diffusion coefficients of CO_2 and CH_4 gases within the membranes, the 13-interval PFG NMR pulse sequence was employed[14,15]. Self-diffusion coefficients were obtained from the PFG NMR attenuation curves, which represent the dependence of the normalized NMR signal intensities on g^2 given by the following equation:[16]

$$\Psi = \frac{S(g)}{S(g \approx 0)} = \exp\left(-q^2 D_s t_{eff}\right) \qquad eq\ 6$$

where D_s is the self-diffusivity, $S(g)$ is the PFG NMR signal intensity at the gradient amplitude g, $q = \gamma \delta g$, and γ is the gyromagnetic ratio corresponding to the nucleus type used. It is important to note that this equation is valid for normal diffusion with a single time-independent self-diffusivity D_s for any species. The activation energies of self-diffusion (E_s) and the pre-exponential factors ($D_{s,0}$) were obtained using the Arrhenius law

$$D_s = D_{s,0} e^{-\frac{E_s}{RT}} \qquad eq\ 7$$

where R is the universal gas constant and T is the absolute temperature. The root mean square displacements (RMSDs) of gas molecules were calculated using the Einstein diffusion equation for three-dimensional diffusion:[17]

$$\langle r^2 \rangle^{1/2} = \sqrt{6 D_s t_{eff}} \qquad eq\ 8$$

The longitudinal (T_1) and transverse (T_2) NMR relaxation times of CO_2 and CH_4 were measured at all three experimental temperatures (35°C, 50°C, and 80°C) using the Inversion recovery pulse sequence and Carr-Purcell-Meiboom-Gill (CPMG) pulse sequence with tau = 0.1 ms, respectively. The obtained T_2 values ranged from approximately 4 to 21 ms for ^{13}C nuclei and from about 8 to 17 ms for ^{1}H nuclei. The ^{13}C T_1 NMR relaxation times were in the range of 0.7 to 1.7 s, and the ^{1}H T_1 NMR relaxation times were in the range of 1.1 to 2.0 s.

Computational simulation

Simulations involve the combination of quantum chemical (QC) calculations with molecular dynamics (MD). The QC calculations involve modelling short oligomers consisting of three repeat units of the polymer capped at both ends to ensure a realistic charge distribution across the chain. Initial geometries were optimized using the semi-empirical GFN2-xTB method as implemented in the xTB package[18]. These geometries were then optimized through density functional theory (DFT) with the B3LYP functional and def2-SVP basis set in Gaussian 16 software package[19] and single-point energy calculation with def2-TZVP basis set to yield a more accurate electronic description. Electrostatic potentials from this calculation were used to generate atom-centered charges via the restrained electrostatic potential (RESP) charge scheme[20] out using Multiwfn[21]. These charges were then used in the MD simulations. The General Amber Force Field (GAFF)[22] was used to model the polymers with chains generated using the *Polymatic* simulated polymerization algorithm[23], which uses a 21-stage equilibration procedure to grow and relax the chains into converged configurations. Short-range interactions were truncated at 14 Å, and electrostatics were handled with the Particle Mesh Ewald (PME) approach with a Fourier grid spacing of 1.2 Å. The temperature and pressure were maintained at 298 K and 1 bar using the Nosé-Hoover thermostat[24] and Parrinello-Rahman barostat[25], respectively. All Simulations were performed in GROMACS[26] with periodic boundaries in all three directions and H-bonds constrained with the LINCS algorithm. Visualization was done with VMD[27]. After polymerization, 10 polymer chains, each containing 20 repeat units and respective ions, were packed and minimized using the steepest descent method. This was followed by 4 annealing cycles, where the system was heated to 750 K and cooled to 298 K over 70 ns per cycle. The final system composition is shown in Fig. S1. The solvent assessable surface area (SASA) and fractional free volume (FFV) analyses were performed using our in-house code, following the methods of Gelb and Gubbins[28], with spherical probe radii of 0.1 nm and 0 nm, respectively. To ensure reproducibility and reliable statistics, each system was simulated in three independent replicas.

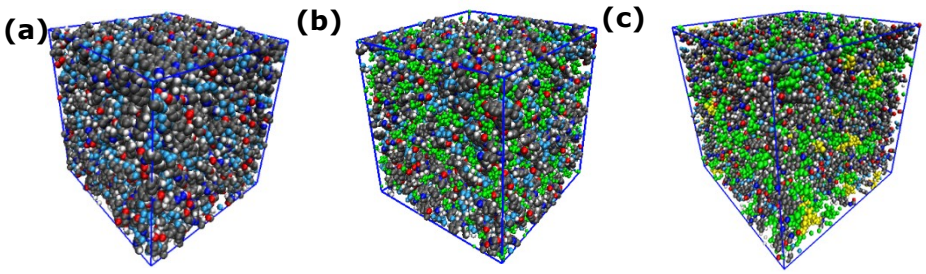

Fig. S1 Visualization of equilibrated polymer structures. (a) PI-(CF_3-Im)-6FDA, (b) PI-(CF_3-Im-Me)-6FDA and (c) PI-(CF_3-Im-Me)-6FDA+IL. The $[TF_2N]^-$ anions are represented in green and the $[BMIM]^+$ cations are represented in yellow.

Regarding the MD simulations, ten independent models were created for each polymer. To obtain each model, a defined quantity of repetitive units was randomly packed into a cubic periodic box, with the edge length depending on the initial packing density. The models of each polymer were created from initial densities of 0.3 g cm^{-3}. The general AMBER force field (GAFF)[22] was used to describe the bonded interactions, while the transferable potentials for phase equilibria with united atoms (TraPPE-UA) force field was used to describe the interactions between non-bonded atom pairs. Atomic charges were calculated with the Gaussian code using the restrained electrostatic potential (RESP) charge scheme[20]. For this, the geometries were optimized using the Hartree-Fock method, representing the wave function with the Pople 6-31G-d Gaussian basis set. The free volume (V_f), defined by the separation between polymer chains, was calculated using the "Atom Volumes and Surfaces" tool from the Materials Studio 7.0 software package[29]. The procedure was based on measuring the surface traced by the edge of a sphere with a radius of 1.65 Å, as reported previously[30], if it were rolled over the surface defined by the atoms in the system according to their van der Waals radii (Connolly surface)[31]. Once the total volume (V) of the cubic unit cell, defined by its edge length, was known, the FFV was determined by calculating the ratio V_f/V.

Film preparation

Pristine polyimide, PI-(CF_3-Im)-6FDA, dense film was prepared from a 10 wt% (w/v) solution in $CHCl_3$ (1 g in 10 mL) by the solution-casting method. The solution was filtered through a 3.1 μm fiberglass Synta® syringe filter and were poured into a circular Teflon® Petri dish placed on a level surface. The solvent was evaporated at room temperature for 48 h. The dense film was peeled off and placed in a vacuum oven at 120 ºC for 24 h. In the case of the ionic polyimide, PI-(CF_3-Im-Me)-6FDA, the procedure was the same but employing DMA as solvent instead chloroform. DMA was evaporated at 60 °C for 48 h, and then the temperature was slowly raised to 150 °C. Finally, for the

ionic polyimide containing IL, PI-(CF_3-Im-Me)-6FDA + IL, DMA was also used as solvent, but the procedure incorporated the addition of 1 equiv. of [C_4mim][Tf_2N] for repeat unit in the ionic polyimide. Photographs of each film are shown in Fig. S2.

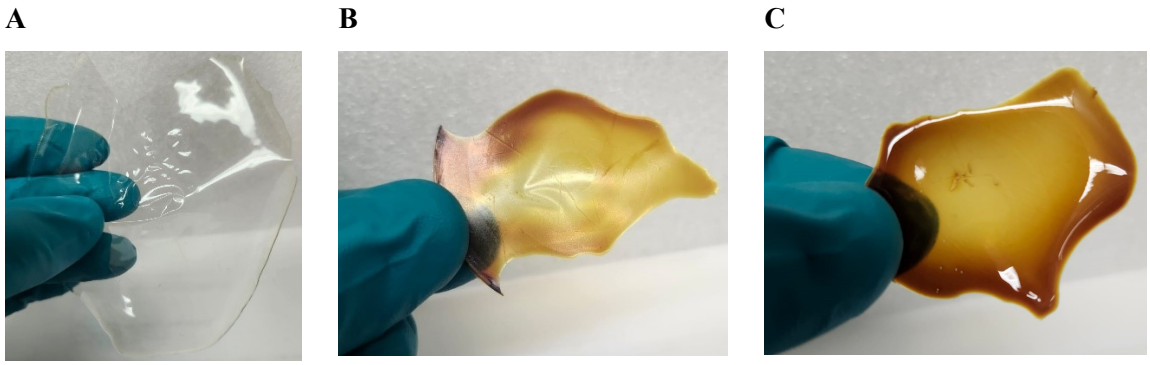

Fig. S2 Dense films prepared from: A) PI-(CF_3-Im)-6FDA. B) PI-(CF_3-Im-Me)-6FDA. C) PI-(CF_3-Im-Me)-6FDA + IL.

Monomer synthesis

*2.5.1. Synthesis of 1,4-bis(4-(trifluoromethyl)-1H-imidazol-2-yl)benzene (**1**).* In a flask were dissolved 14.4 g (0.176 mol) of sodium acetate (NaOAc) in 80 mL of H_2O, and then 23.7 g (0.088 mol) of 3,3-dibromo-1,1,1-trifluoropropan-2-one were added slowly under stirring until complete dissolution. The contents of the flask were put into an isobaric funnel that was connected to a 1000 mL two-necked round bottom flask, which contained 5.36 g (0.040 mol) of terephthalaldehyde dissolved in 400 mL of MeOH and 100 mL of NH_4OH solution (25%). The isobaric funnel was allowed to drop until empty for 30 min. A yellow precipitate appeared after 10 min of the addition, but it disappeared almost completely after stirring overnight at RT. The mixture was filtered under gravity to remove any solid content, and it was concentrated by rotavapor until haft the original volume. At that time, a yellow solid appeared, which was filtered under reduced pressure. (Note: do not concentrate until dryness). The solid was thoroughly washed with H_2O and dried at 80 °C overnight. The solid was further purified by trituration in 100 mL of hot EtOAc and collected via vacuum filtration. Finally, it was dried at 80 °C in an oven.

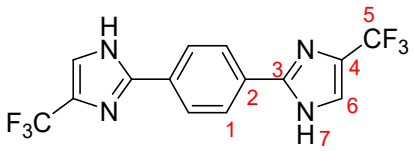

1: Yield: 60%. M.p.: > 300 ºC. ATR-IR (υ, cm^{-1}): 3187 – 2272 (Broad band N-H, C_{Im}-H and C-H phenyl); 1593, 1567, 1484, 1446 (C=C and C=N); 1355 (C-N); 1106 (CF_3). ^{1}H NMR (DMSO-d_6, δ, ppm): 13.30 (s, 2H, H7); 8.10 (s, 4H, H1); 7.96 (s, 2H, H6). ^{13}C NMR (DMSO-d_6, δ, ppm): 147.20

(C3); 131.81, 131.50, 131.20, 130.90 (q, ^{2}J = *37.29 Hz*, C4); 130.23 (C2); 126.29 (C1); 119.71 (C6); 125.92, 123.80, 121.68, 119.56 (q, *J= 266.30 Hz*, C5). ^{19}F NMR (DMSO-d_6, δ, ppm): -60.75 (CF_3).

*2.5.2. Synthesis of 1,4-bis(1-(4-nitrophenyl)-4-(trifluoromethyl)-1H-imidazol-2-yl)benzene (**2**).* In a one-necked flask equipped with magnetic stirring was added 8.0 g (0.023 mol) of **1**, 7.14 g (0.050 mol) of 1-fluoro-4-nitrobenzene, 9.54 g (0.069 mol) of K_2CO_3 and 40 mL of DMSO. The mixture was heated at 105 °C overnight, and then it was poured into 350 mL of DI water under stirring. The yellow solid was recovered by filtration and washed with water, and then with EtOH.

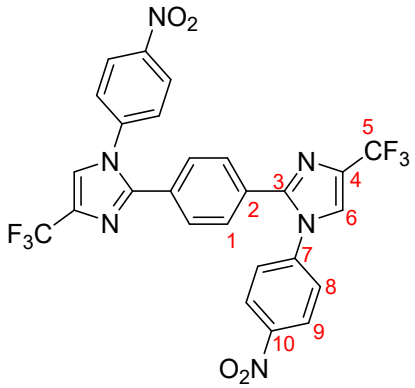

2: Yield: 75%. M.p.: > 300 ºC. ATR-IR (υ, cm^{-1}): 3161, 3115, 3079, 3052, 2997 (C_{Im}-H and C-H phenyl); 1598, 1579, 1498, 1470, 1425 (C=C and C=N); 1520 (symmetrical Ar-NO_2); 1363 (C-N); 1348 (Ar-NO_2 asymmetric); 1125 (CF_3). ^{1}H NMR (DMSO-d_6, δ, ppm): 8.41 (s, 2H, H6); 8.32 (d, *J = 9.0 Hz*, 4H, H9); 7.66 (d, *J = 9.0 Hz*, 4H, H8); 7.34 (s, 4H, H1). ^{13}C NMR (DMSO-d_6, δ, ppm): 147.65 (C10); 147.08 (C3); 142.19 (C7); 131.76, 131.44, 131.13, 130.81 (q, ^{2}J = *38.52 Hz*, C4); 129.77 (C2); 129.49 (C1); 127.95 (C9); 125.33 (C8); 124.64 (C6); 127.60, 125.46, 123.34, 121.22 (q, *J= 266.36 Hz*, C5). ^{19}F NMR (DMSO-d_6, δ, ppm): -61.33 (CF_3).

*2.5.3. Synthesis of 4,4'-(1,4-phenylenebis(4-(trifluoromethyl)-1H-imidazole-2,1-diyl))dianiline (**3**).* In a 250 mL two-necked flask equipped with magnetic stirring was added 10 g (0.017 mol) of the dinitro precursor (**2**), 1.0 g of Pd/C (10%), 100 mL of HFIP and 30 mL of EtOH. The reaction was heated at reflux, and 10 mL of hydrazine hydrate ($N_2H_4.H_2O$ 98%) was dropped over a period of 30 min. Then, the mixture heated at reflux for 5 h. Once cooled to RT, the reaction was filtered over a pad of Celite, and the solvent was removed by reduced pressure in a rotary evaporator. The solid was washed with water and dried at 80 °C in an oven for 24 h. Recrystallization from MeOH yielded the product as a white-off solid.

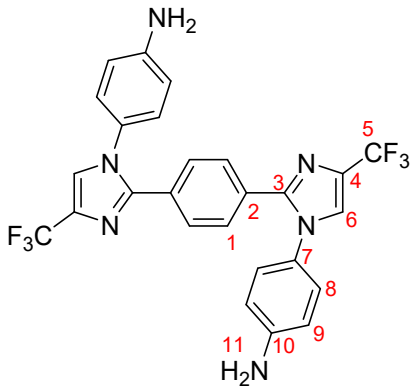

3: Yield: 95%. M.p.: 294 - 296 ºC. ATR-IR (υ, cm^{-1}): 3480, 3353, 3228 (N-H); 3124, 3048, 2980 (C_{Im}-H and C-H phenyl); 1635, 1610 (N-H flexion); 1574, 1521, 1470, 1431 (C=C and C=N); 1362 (C-N); 1112 (CF_3). ^{1}H NMR (DMSO-d_6, δ, ppm): 8.03 (s, 2H, H6); 7.32 (s, 4H, H1); 6.98 (d, *J = 8.7 Hz*, 4H, H8); 6.59 (d, *J = 8.7 Hz*, 4H, H9); 5.48 (s, 4H, H11). ^{13}C NMR (DMSO-d_6, δ, ppm): 149.97 (C3); 146.90 (C10); 130.75, 130.44, 130.13, 129.83 (q, ^2J *= 38.61 Hz*, C4); 130.05 (C2); 128.48 (C1); 127.34 (C8); 125.38 (C7); 125.08 (C6); 125.72, 123.59, 121.47, 119.36 (q, *J= 266.58 Hz*, C5); 114.29 (C9). ^{19}F NMR (DMSO-d_6, δ, ppm): -60.94 (CF_3).

Synthesis of polyimides

2.6.1. PI-(CF_3-Im)-6FDA. In a 3-necked round-bottom flask, 2.0000 g (3.78 mmol) of the diamine monomer (**3**) were dissolved in anh. DMAc (4.0 mL), and the reaction mixture was cooled in a water-ice bath. Then, 1.6792 g (3.78 mmol) of freshly sublimed 6FDA were added followed by 4.0 mL of anh. DMAc. The mixture was kept with constant mechanical stirring under a N_2 atmosphere at 0 °C until complete dissolution of the reactants. Then, the mixture was allowed to reach room temperature (RT), and after 5 h, 1.5 mL (19 mmol) of anh. Py and 1.8 mL (19 mmol) of anh. Ac_2O were added. The solution was stirred at RT for 2 h. Finally, the temperature was gradually increased to 60 °C for 1 h. The resulting solution was poured into water, and the solid was collected by filtration. The polymer was dried at 80 °C in a vacuum oven. The dried polyimide (3.5 g) was dissolved in $CHCl_3$ (25 mL), and it was re-precipitated by slowly dropping MeOH (< 25 mL) to purify and remove oligomeric chains. The final solids were dried in a vacuum oven at 80 °C to remove any volatile components.

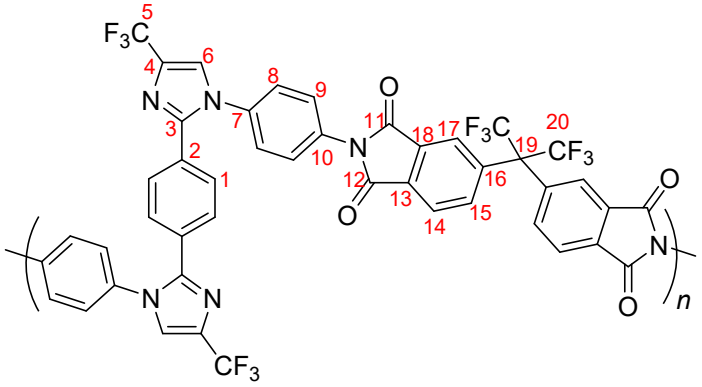

PI-(CF_3-Im)-6FDA: ATR-IR (υ, cm^{-1}): 3122, 3073, 2982, 2927, 2855 (C_{Im}-H and C-H phenyl); 1788, 1723 (C=O imide); 1578, 1517, 1466 (C=C and C=N); 1359 (C-N); 1116 (C-F); 719 (bending imide ring). ^{1}H NMR (DMSO-d_6, δ, ppm): 8.33 (s, 2H, H6); 8.14 (broad, 2H, H15); 7.95 (broad, 2H, H14); 7.76 (s, 2H, H17); 7.57 (s, 8H, H8 and H9); 7.37 (s, 4H, H1). ^{19}F NMR (DMSO-d_6, δ, ppm): -61.20 (CF_3); -62.89 (F-6FDA).

2.6.2. PI-(CF_3-Im-Me)-6FDA. In a 100 mL pressure vessel was dissolved 1 g of PI-(CF_3-Im)-6FDA in 10 mL of DMSO. Subsequently, 0.45 mL (7 eq.) of MeI was added, and the vessel was closed. The reaction was kept at 80 °C under stirring for 24 h. Then, the reaction mixture was poured into 300 mL of DI water under stirring, the solid was filtered, washed with plenty of water, and dried at 80 °C for 24 h. Then, the ionic polyimide (1.2 g) was dissolved in 10 mL of acetone and was dropped into a solution of 1.8 g (6 eq.) of $LiTf_2N$ in 20 mL of acetone. After complete addition, the mixture was left to stir for 30 min, and then it was poured over 250 mL of DI water under stirring. The solid was recovered by filtration, washed with water, and dried at 80 °C for 24 h under vacuum. Finally, the solid was suspended in $CHCl_3$ under stirring for 30 min, filtered, and washed with $CHCl_3$ to remove any unreacted chains or chains with a low content of ionic fragments.

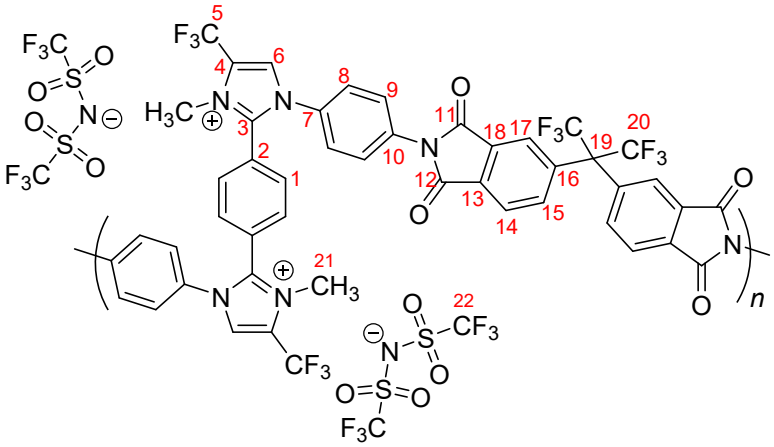

PI-(CF_3-Im-Me)-6FDA: ATR-IR (υ, cm^{-1}): 3155, 3118, 2982, 2969, 2934, 2880 (C_{Im}-H, C-H phenyl and C-H aliph.); 1787, 1724 (C=O imide); 1576, 1519, 1467, 1428 (C=C and C=N); 1352 (C-N); 1331, 1187 (SO_2); 1127 (C-F); 1051 (S-N-S); 721 (bending imide ring). ^{1}H NMR (DMSO-d_6, δ, ppm): 8.33 (s, 2H H6); 8.14 (broad, 2H, H15); 7.95 (broad, 2H, H14); 7.75 (broad, 2H, H17); 7.57 (s, 8H, H8 and H9); 7.37 (s, 4H, H1); 3.83 (s, 6H, H21). ^{19}F NMR (DMSO-d_6, δ, ppm): -61.19 (CF_3); -62.89 (F-6FDA); -78.72 (F-NTf_2).

Additional Figures

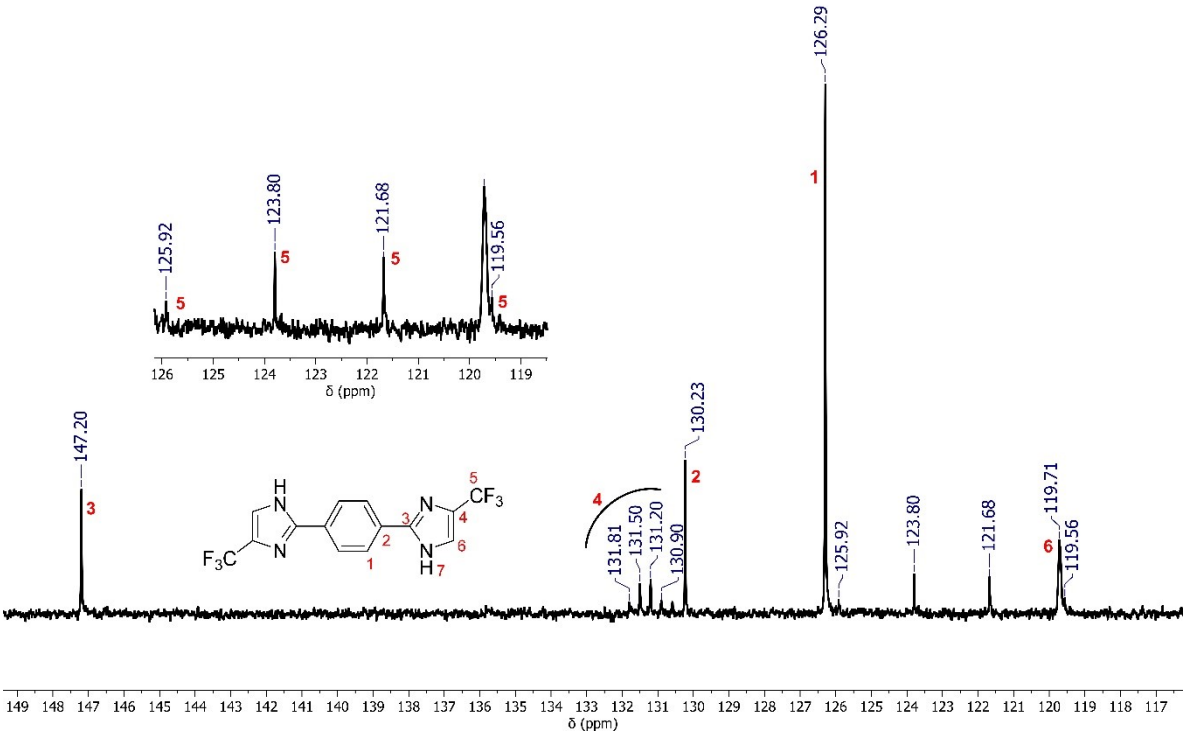

Fig. S3 Full assignment of ^{13}C NMR spectra in DMSO-d_6 of compound 1.

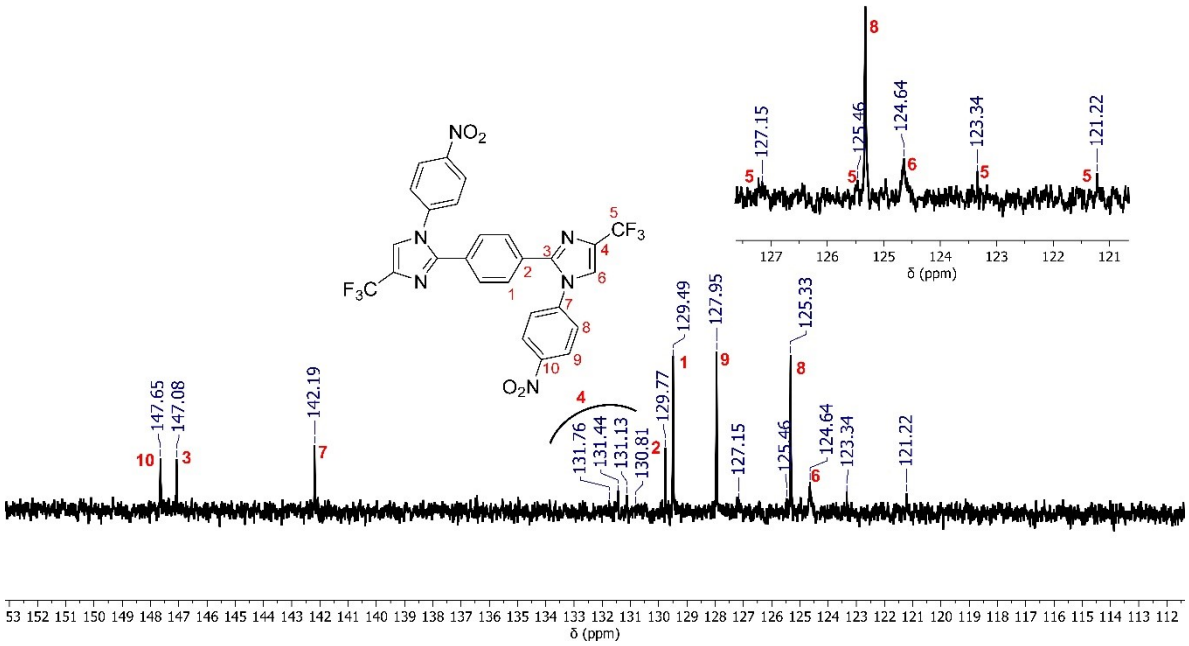

Fig. S4 Full assignment of ^{1}H NMR spectra in DMSO-d_6 of compound 2.

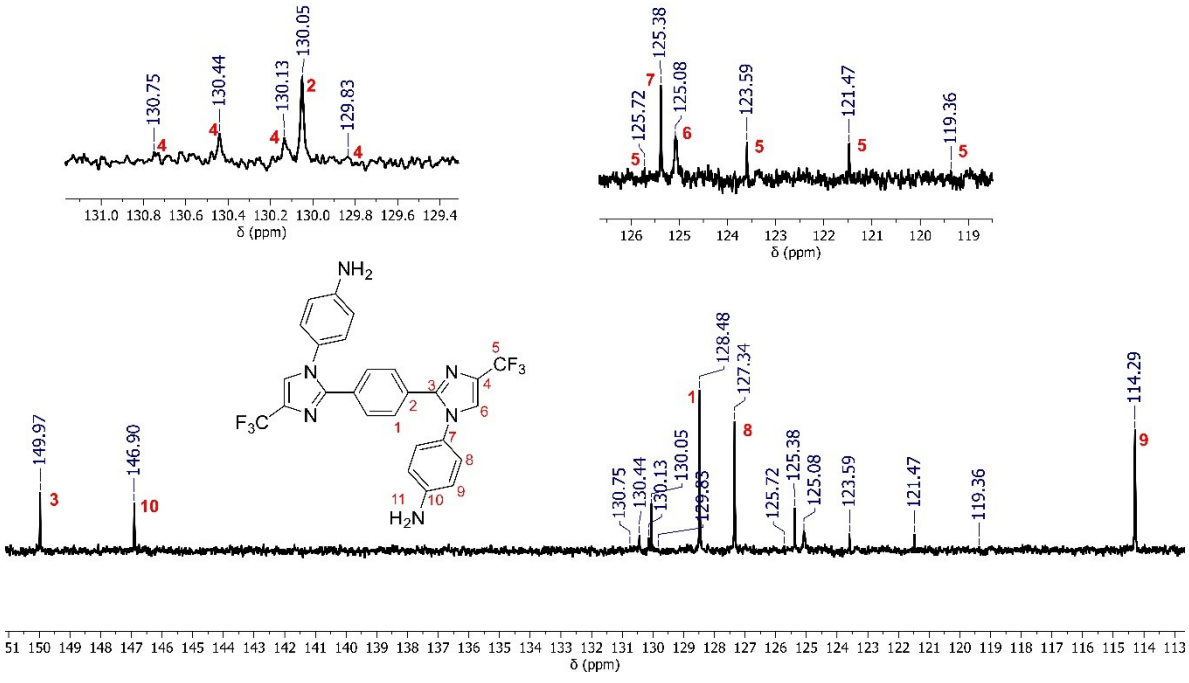

Fig. S5 Full assignment of ^{13}C NMR spectra in DMSO-d_6 of compound 4.

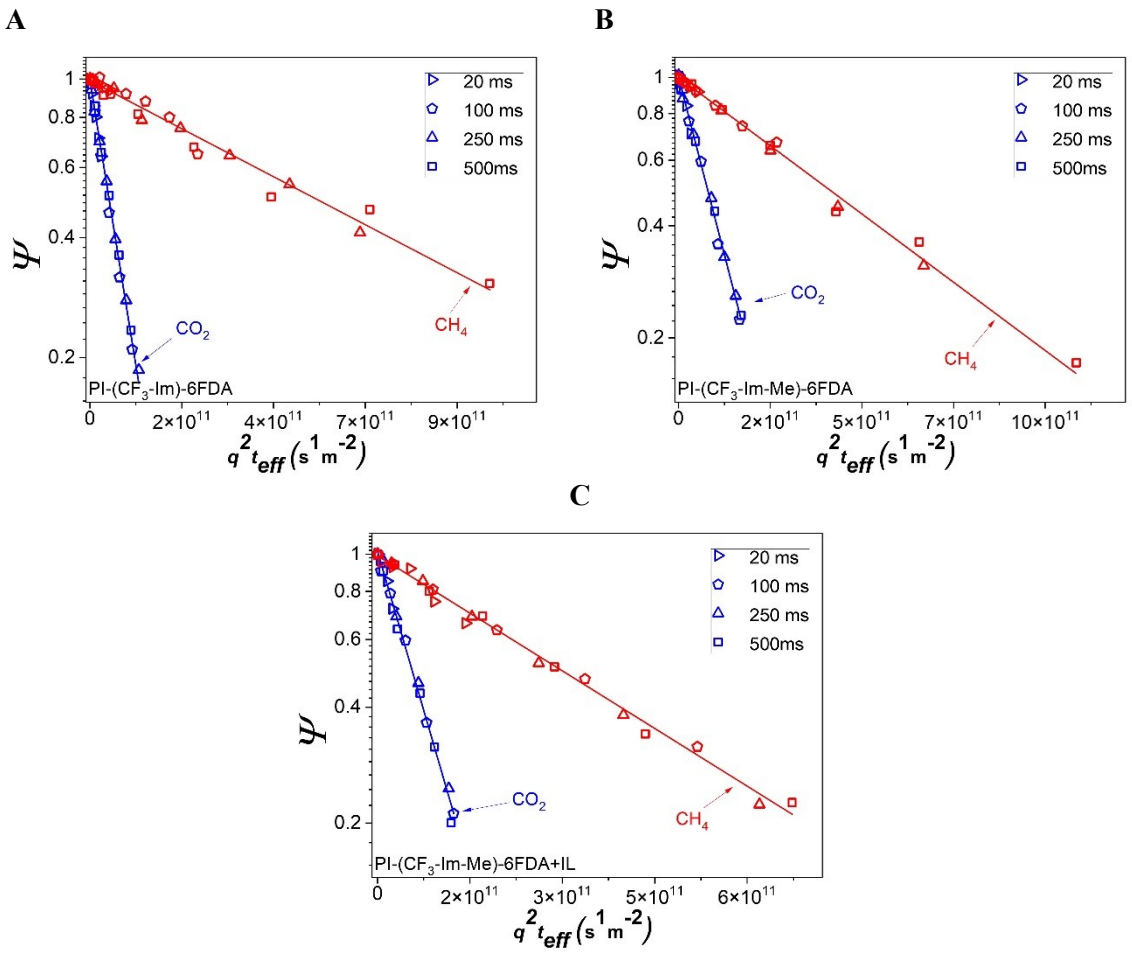

Fig. S6 PFG NMR attenuation curves measured at 50 °C for one-component CO_2 or CH_4 at different effective diffusion times for A) PI-(CF_3-Im)-6FDA, B) PI-(CF_3-Im-Me)-6FDA, and C) PI-(CF_3-Im-Me)-6FDA + IL membranes. Hollow points and filled points indicate data obtained using ^{13}C and ^{1}H, respectively. The straight lines represent best-fit lines using Eq. 6.

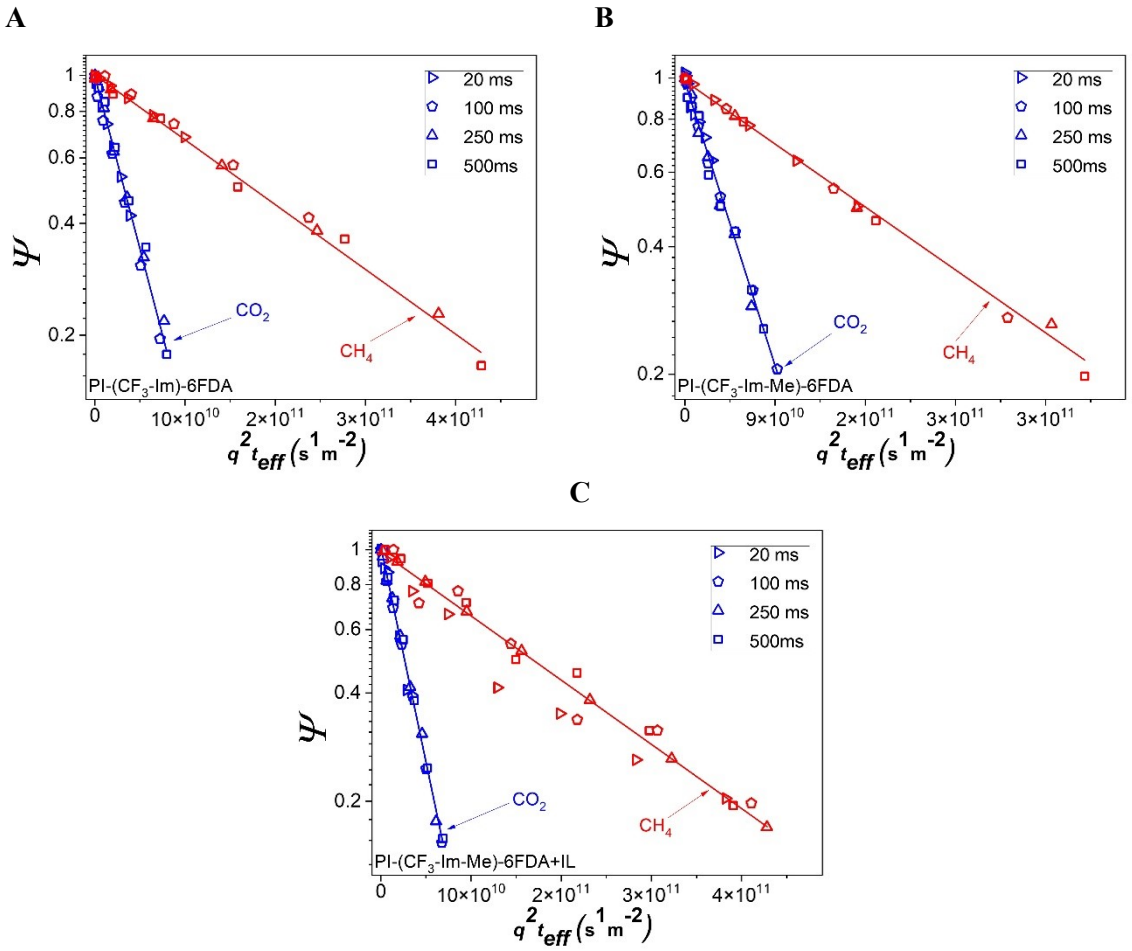

Fig. S7 PFG NMR attenuation curves measured at 80 °C for one-component CO_2 or CH_4 at different effective diffusion times for A) PI-(CF_3-Im)-6FDA, B) PI-(CF_3-Im-Me)-6FDA, and C) PI-(CF_3-Im-Me)-6FDA + IL membranes. Hollow points and filled points indicate data obtained using ^{13}C and ^{1}H, respectively. The straight lines represent best-fit lines using Eq. 6.

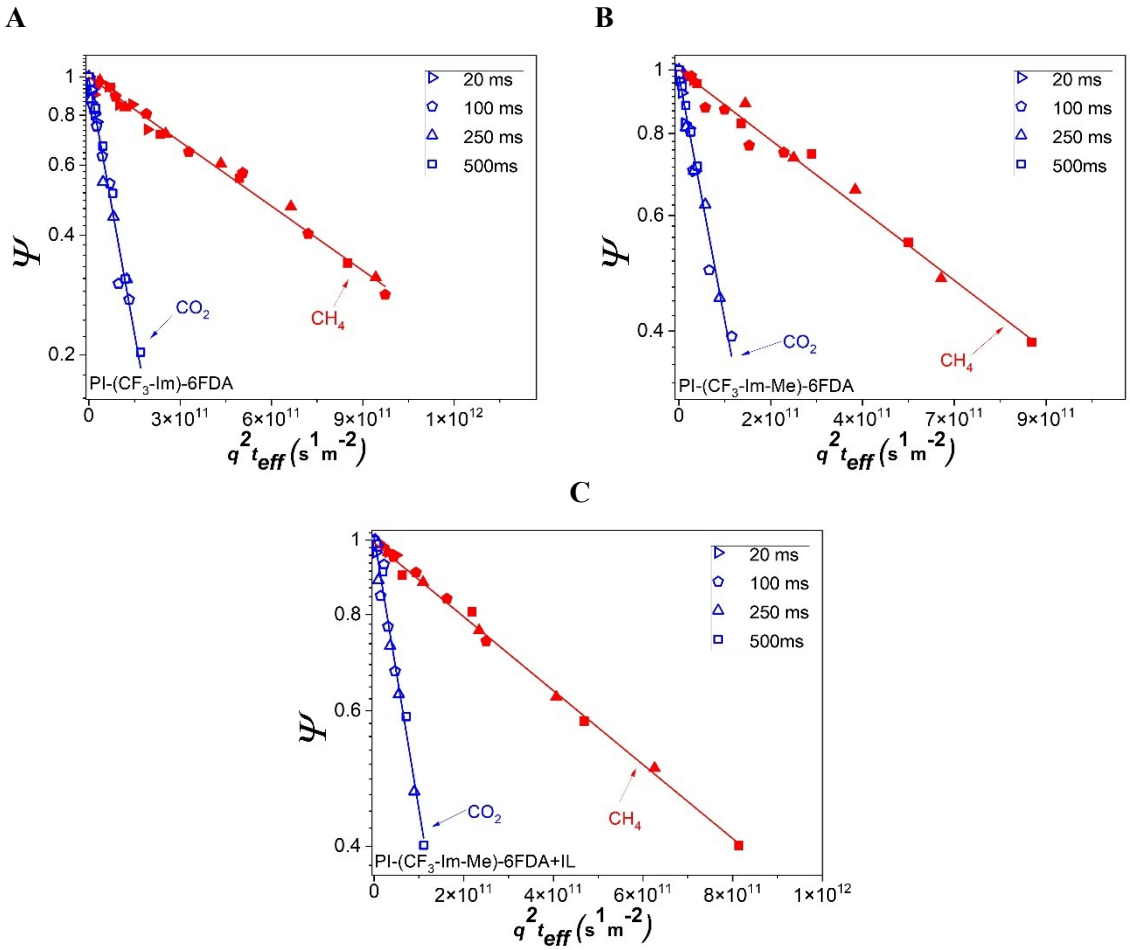

Fig. S8 PFG NMR attenuation curves measured at 35 °C for two-component gas mixture containing CO_2 and CH_4 at different effective diffusion times for A) PI-(CF_3-Im)-6FDA, B) PI-(CF_3-Im-Me)-6FDA, and C) PI-(CF_3-Im-Me)-6FDA + IL membranes. Hollow points and filled points indicate data obtained using ^{13}C and ^{1}H, respectively. The straight lines represent best-fit lines using Eq. 6.

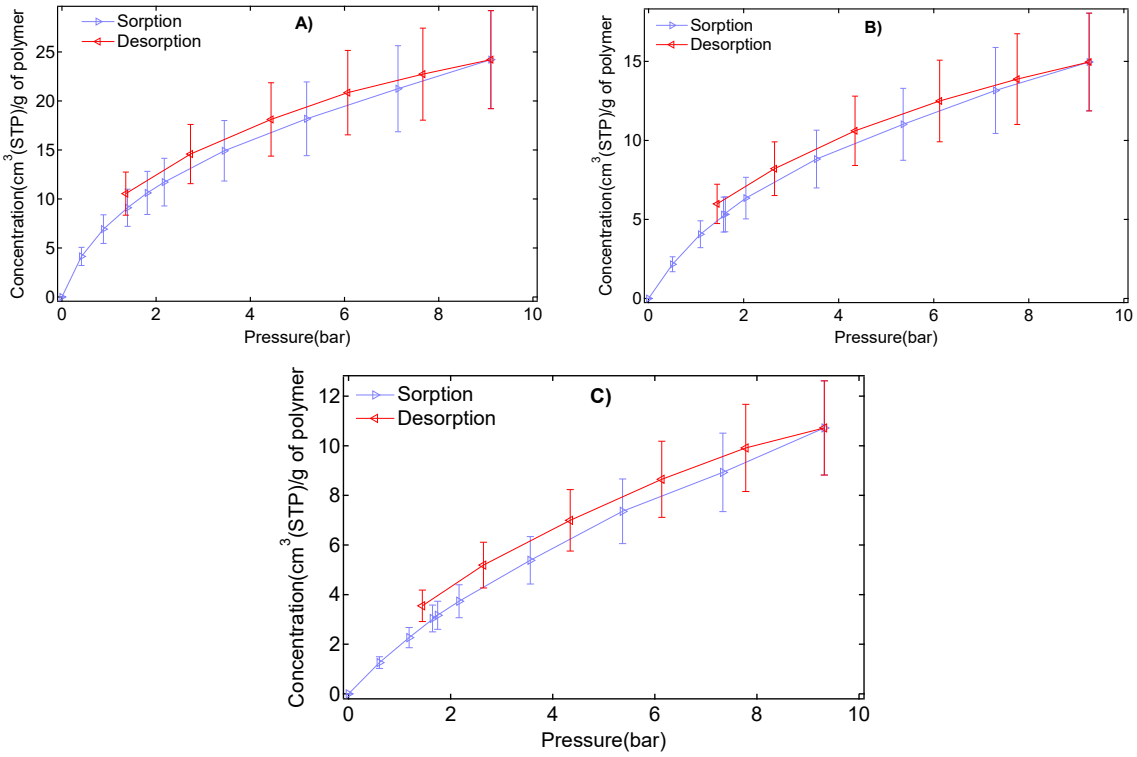

Fig. S9 Sorption-desorption hysteresis plots of CO_2 for A) PI-(CF_3-Im)-6FDA, B) PI-(CF_3-Im-Me)-6FDA, and C) PI-(CF_3-Im-Me)-6FDA + IL membranes.

Additional tables

Table S1 One-component CO_2 gas loading pressures and concentration within the membrane for the NMR samples at different temperatures.

Membrane	Temperature of the measurement (°C)	Pressure in gas phase (bar)*	Concentration of gas adsorbed within the membrane (mmol/g)[#]
PI-(CF_3-Im)-6FDA	35	9.3	1.5
	50	9.2	1.4
	80	9.4	1.2
PI-(CF_3-Im-Me)-6FDA	35	9.8	0.96
	50	9.8	0.91
	80	9.9	0.72
PI-(CF_3-Im-Me)-6FDA + IL	35	9.8	0.53
	50	9.9	0.49
	80	9.9	0.41

*15% experimental uncertainty
[#]20% experimental uncertainty

Table S2 One-component CH_4 gas loading pressures and concentration within the membrane for the studied NMR samples at different temperatures.

Membrane	Temperature of the measurement (°C)	Pressure in gas phase (bar)*	Concentration of gas adsorbed within the membrane (mmol/g)[#]
PI-(CF_3-Im)-6FDA	35	9.8	0.18
	50	9.8	0.15
	80	9.9	0.10
PI-(CF_3-Im-Me)-6FDA	35	9.7	0.17
	50	9.8	0.14
	80	9.8	0.10
PI-(CF_3-Im-Me)-6FDA + IL	35	10	0.21
	50	10	0.18
	80	10	0.15

*15% experimental uncertainty
[#]20% experimental uncertainty

Table S3 Two-component CO_2 and CH_4 gas loading pressures and concentrations within the membrane for the NMR samples at 35 °C.

Membrane	Pressure in gas phase (bar)*		Concentration of gas adsorbed within the membrane (mmol/g)#		Total pressure in gas phase (bar)*	Total concentration of gas adsorbed in two-component sample (mmol/g)#
	CO_2	CH_4	CO_2	CH_4		
PI-(CF_3-Im)-6FDA	7.1	2.8	1.0	0.070	10	1.05
PI-(CF_3-Im-Me)-6FDA	7.1	3.0	0.70	0.060	10	0.76
PI-(CF_3-Im-Me)-6FDA + IL	7.3	2.9	0.35	0.060	10	0.41

*15% experimental uncertainty
#20% experimental uncertainty

Table S4 PFG NMR self-diffusion data for one-component gases in the membranes along with their corresponding ranges of RMSDs and self-diffusion selectivities.

Sorbate	Membrane	Temperature of the measurement (°C)	Range of t_{eff} (ms)	$D_s \times 10^8$ (cm^2/s)	Range of root MSDs (μm)	Self-diffusion selectivity ($D_{s,CO_2}/D_{s,CH_4}$)*
CO_2	PI-(CF_3-Im)-6FDA	35	20 – 500	9.8 ± 1	1.1 ± 0.1 – 5.4 ± 0.5	10.9
		50	20 – 500	13 ± 1	1.4 ± 0.1 – 6.9 ± 0.7	9.2
		80	20 – 500	22 ± 2	1.6 ± 0.2 – 8.1 ± 0.8	5.9
	PI-(CF_3-Im-Me)-6FDA	35	20 – 500	7.9 ± 0.8	1.0 ± 0.1 – 4.9 ± 0.5	7.0
		50	20 – 500	9.3 ± 1	1.2 ± 0.1 – 5.1 ± 0.5	4.7
		80	20 – 500	18 ± 2	1.4 ± 0.1 – 7.3 ± 0.7	4.3
	PI-(CF_3-Im-Me)-6FDA + IL	35	20 – 500	8.2 ± 0.8	1.0 ± 0.1 – 4.9 ± 0.5	6.8
		50	20 – 500	12 ± 1	1.2 ± 0.1 – 6.0 ± 0.6	5.4
		80	20 – 500	29 ± 3	1.9 ± 0.2 – 9.4 ± 0.9	6.7
CH_4	PI-(CF_3-Im)-6FDA	35	20 – 500	0.9 ± 0.1	0.3 ± 0.03 – 1.7 ± 0.2	10.9
		50	20 – 500	1.4 ± 0.1	0.4 ± 0.04 – 2.0 ± 0.2	9.2
		80	20 – 500	3.7 ± 0.4	0.7 ± 0.07 – 3.5 ± 0.4	5.9
	PI-(CF_3-Im-Me)-	35	20 – 500	1.1 ± 0.1	0.4 ± 0.04 – 2.0 ± 0.2	7.0

	6FDA	50	20 – 500	2.0 ± 0.2	0.5 ± 0.05 – 2.3 ± 0.2	4.7
		80	20 – 500	4.2 ± 0.4	0.7 ± 0.07 – 3.6 ± 0.4	4.3
	PI-(CF_3-Im-Me)-6FDA + IL	35	20 – 500	1.2 ± 0.1	0.4 ± 0.04 – 2.0 ± 0.2	6.8
		50	20 – 500	2.0 ± 0.2	0.5 ± 0.05 – 2.6 ± 0.3	5.4
		80	20 – 500	4.3 ± 0.4	0.7 ± 0.07 – 3.6 ± 0.4	6.7

*20% experimental uncertainty

Table S5 PFG NMR self-diffusion data for two-component gas mixture of CO_2 and CH_4 in the NMR samples along with their corresponding self-diffusion selectivities at 35 °C.

Membrane	Range of t_{eff} (ms)	$D_s \times 10^8$ (cm²/s)		Self-diffusion selectivity ($D_{s,CO_2}/D_{s,CH_4}$)*
		CO_2	CH_4	
PI-(CF_3-Im)-6FDA	20 – 500	9.9 ± 1	1.2 ± 0.1	8.2
PI-(CF_3-Im-Me)-6FDA	20 – 500	7.8 ± 0.8	1.1 ± 0.1	7.0
PI-(CF_3-Im-Me)-6FDA+ IL	20 – 500	7.8 ± 0.8	1.0 ± 0.1	7.1

*20% experimental uncertainty

References for Supporting Information

1 J. E. Bara, C. J. Gabriel, S. Lessmann, T. K. Carlisle, A. Finotello, D. L. Gin and R. D. Noble, *Ind. Eng. Chem. Res.*, 2007, **46**, 5380–5386.
2 D. Camper, J. E. Bara, D. L. Gin and R. D. Noble, *Ind. Eng. Chem. Res.*, 2008, **47**, 8496–8498.
3 S. Ravula, K. W. Wise, P. S. Shinde and J. E. Bara, *Macromolecules*, 2023, **56**, 6126–6141.
4 N. S. Murthy, in *Polymer Morphology: Principles, Characterization, and Processing*, 2016.
5 H. Czichos, T. Saito and L. Smith, Eds., *Springer Handbook of Materials Measurement Methods*, Springer Berlin Heidelberg, Berlin, Heidelberg, 2006.
6 H. Lin and B. D. Freeman, *Macromolecules*, 2005, **38**, 8394–8407.
7 E. Ricci, F. M. Benedetti, M. E. Dose, M. G. De Angelis, B. D. Freeman and D. R. Paul, *J. Memb. Sci.*, 2020, **612**, 118374.
8 J. S. Sengers, J. M. H. L.; Klein, M.; Gallagher, *Pressure-Volume-Temperature Relationships of Gases Virial Coefficients*, 1971.
9 R. A. Johnson, Z. Reddecliff, K. El Hajj Sleiman and J. D. Moon, *J. Memb. Sci.*, 2025, **722**, 123825.
10 R. Mueller, S. Zhang, C. Zhang, R. Lively and S. Vasenkov, *J. Memb. Sci.*, 2015, **477**, 123–130.
11 S. Ravula, F. E. Rodríguez-González, P. S. Shinde, A. L. Montero-Alejo, C. A. Terraza, S. Laxmi, S. Vasenkov, K. E. O'Harra, A. Tundidor-Camba and J. E. Bara, *Macromolecules*, 2024, **57**, 11085–11096.
12 R. Span and W. Wagner, *J. Phys. Chem. Ref. Data*, 1996, **25**, 1509–1596.
13 U. Setzmann and W. Wagner, *J. Phys. Chem. Ref. Data*, 1991, **20**, 1061–1155.
14 R. . Cotts, M. J. . Hoch, T. Sun and J. . Markert, *J. Magn. Reson.*, 1989, **83**, 252–266.
15 S. J. Gibbs and C. S. Johnson, *J. Magn. Reson.*, 1991, **93**, 395–402.
16 J. Kärger, D. M. Ruthven and D. N. Theodorou, *Diffusion in Nanoporous Materials*, Wiley, 2012.
17 In *Diffusion in Nanoporous Materials*, Wiley, 2012, pp. 347–394.
18 C. Bannwarth, E. Caldeweyher, S. Ehlert, A. Hansen, P. Pracht, J. Seibert, S. Spicher and S. Grimme, *WIREs Comput. Mol. Sci.*, DOI:10.1002/wcms.1493.

19 et al. Frisch MJ, Trucks GW, Schlegel HB, Scuseria GE, Robb MA, Cheeseman JR, 2016.
20 and D. J. F. M. J. Frisch, G. W. Trucks, H. B. Schlegel, G. E. Scuseria, M. A. Robb, J. R. Cheeseman, G. Scalmani, V. Barone, G. A. Petersson, H. Nakatsuji, X. Li, M. Caricato, A. Marenich, J. Bloino, B. G. Janesko, R. Gomperts, B. Mennucci, H. P. Hratchian, J. V. Ort, 2016.
21 T. Lu and F. Chen, *J. Comput. Chem.*, 2012, **33**, 580–592.
22 J. Wang, R. M. Wolf, J. W. Caldwell, P. A. Kollman and D. A. Case, *J. Comput. Chem.*, 2004, **25**, 1157–1174.
23 L. J. Abbott, K. E. Hart and C. M. Colina, *Theor. Chem. Acc.*, 2013, **132**, 1334.
24 S. Nosé, *J. Chem. Phys.*, 1984, **81**, 511–519.
25 M. Parrinello and A. Rahman, *J. Appl. Phys.*, 1981, **52**, 7182–7190.
26 D. Van Der Spoel, E. Lindahl, B. Hess, G. Groenhof, A. E. Mark and H. J. C. Berendsen, *J. Comput. Chem.*, 2005, **26**, 1701–1718.
27 W. Humphrey, A. Dalke and K. Schulten, *J. Mol. Graph.*, 1996, **14**, 33–38.
28 L. D. Gelb and K. E. Gubbins, *Langmuir*, 1999, **15**, 305–308.
29 M. S. BIOVIA, Dassault Systèmes, 2022, [22.1.0.34462].
30 G. Genduso, B. Ghanem, Y. Wang and I. Pinnau, *Polymers (Basel).*, 2019, **11**, 361.
31 M. L. Connolly, *J. Appl. Crystallogr.*, 1983, **16**, 548–558.